Assessing implications of nanoplastics exposure to plants with advanced nanometrology techniques

Ana Elena Pradas del Real, Denise M Mitrano, Hiram Castillo-Michel, Mohammad Wazne, Juan Reyes Herrera, Emely Bortel, Bernhard Hesse, Julie Villanova, Geraldine Sarret

Assessing implications of nanoplastics exposure to plants with advanced nanometrology techniques

Ana Elena Pradas del Real*[1,3], Denise M. Mitrano[2], Hiram Castillo-Michel[3], Mohammad Wazne[3,5], Juan Reyes-Herrera[3], Emely Bortel[4], Bernhard Hesse[3,4], Julie Villanova[3], Géraldine Sarret[5]

1 IMIDRA (Madrid Institute for Agroenvironmental Research). 28800 Alcalá de Henares. Spain

2 ETH Zurich, Universitatstrasse 16, 8092 Zurich, Switzerland

3 ESRF, The European Synchrotron, CS 4022038043 Grenoble Cedex 9, France

4 Xploraytion GmbH, Bismarckstrasse 10-12, 10625, Berlin, Germany

5 ISTerre (Institut des Sciences de la Terre), Univ. Grenoble Alpes, CNRS, 38000

Abstract

Despite the increasing attention given to the impacts of nanoplastics in terrestrial environments, there is limited data about the effects on plants, and the quantitative information on uptake. In the present study, wheat plants grown in hydroponics were exposed to Pd-doped nanoplastics. This allowed us to quantify nanoplastics uptake and translocation to the shoots. Visualization of nanoplastics in roots was performed with synchrotron micro X-ray fluorescence (µXRF). Nanoplastics accumulated on the root epidermis, especially at the root tip and in root maturation zones. A close relationship between plant roots, rhizodeposits and nanoplastics behaviour was shown. Reinforcement of the cell wall in roots was evidenced using Fourier transform infrared spectroscopy (FTIR) and synchrotron-computed microtomography (µCT). Synchrotron-computed nanotomography (nanoCT) evidenced the presence of globular structures but they could not be identified as nanoplastics since they were observed both in the control and treated roots. By utilizing the inorganic tracer in the doped-nanoplastics, this study paves the road for elucidating interactions in more complex systems by using an integrative approach combining classical phytotoxicity markers with advanced nanometrology techniques.

Keywords: quantification, microscopy, cell wall, root anatomy.

Abbreviations: X-ray fluorescence (µXRF), Fourier transform infrared spectroscopy (FTIR), synchrotron-computed microtomography (µCT), ynchrotron-computed nanotomography (nanoCT), scanning electron microscopy (SEM), inductively coupled plasma mass spectrometry (ICP-MS), pyrolysis gas chromatography–mass spectrometry (Py-GC/MS), polystyrene (PS), polyacrylonitrile (PAN), dynamic light scattering (DLS), thermogravimetric analysis (TGA), total organic carbon (TOC), low weight organic acids (LWOAs), instrument limit of detection (LOD), contrast transfer function approach (CTF), linear discriminant analysis (LDA), principal component analysis (PCA), least absolute shrinkage selection operator (LASSO), area under curve (AUC) receiver operating characteristic (ROC), Inorganic engineered nanoparticles (ENPs).

1. Introduction

As industrialization and population growth continue to place increasing pressures on the natural environment, there has been an increased awareness that careful (re)use of our resources are necessary to secure adequate food and water supplies, as highlighted by e.g. the U.N. Sustainable Development Goals(Kanter et al., 2018). Soil nutrient quality and function are fundamental for productive agricultural systems, yet several current strategies to promote nutrient cycling or decrease water usage inadvertently introduce materials into the soil, such as nano- and microplastics. This is notable the case of the reuse of processed sewage sludge as agricultural fertilizer(Kelessidis and Stasinakis, 2012) and the use of plastics in plastic mulch films, greenhouse materials and soil conditioners (Ng et al., 2018; Steinmetz et al., 2016). Atmospheric deposition onto land also contributes to plastic contamination (Bergmann et al., 2019). Data on particulate plastic concentrations in soils is still scarce and differ by several orders of magnitude for microplastics (from a few to a few thousands of $mg \cdot kg^{-1}$ and/or $particles \cdot kg^{-1}$ depending on the studies) (Corradini et al., 2019; Scheurer and Bigalke, 2018; Wu et al., 2021; Zhang and Liu, 2018). The occurrence of nanoplastics in a natural soil has only recently been proved (Wahl et al., 2021) and information about their concentrations is not yet available. The synthetic nature and persistence of particulate plastics may qualify these particles to be drivers of environmental change, but holistically the impacts to both soil quality and plant growth and productivity have only recently begun to be investigated (Chae and An, 2018; Horton et al., 2017; Rillig et al., 2019; Rillig and Lehmann, 2020; Wu et al., 2021). Literature regarding the interaction of plants with plastic debris is still scarce, but there is an increasing number of studies being focussed on the effects caused by nanoplastics in plants.

A recent article demonstrated that microplastics can enter the root of wheat and lettuce(Li et al., 2020). Nanoplastics particles may have a greater potential to cross plant barriers. Indeed, studies have shown that a large number of nanoplastics can enter roots(Jiang et al., 2019; Sun et al., 2020) and be transported to the aerial parts of plants(Chae and An, 2020; Li et al., 2020; Lian et al., 2020; Liu et al., 2022; Zhang et al., 2019a). However, uptake and transport mechanisms are still unclear and quantitative information is really limited, which is key to assess environmental impact and potential risk to human health. Root tips have been identified as one of the main points of entry(Jiang et al., 2019; Lian et al., 2020; Liu et al., 2022; Zhang et al., 2019a), root hairs and the epidermis of maturation zone of roots have also been proposed (Sun et al., 2020). Once inside the plant, apoplastic pathway seems to be the main transport mechanism (Li et al., 2020; Liu et al., 2022; Sun et al., 2020), although the symplastic pathway cannot be excluded with the available data. To date, only one study has quantified nanoplastics in plant tissues. The authors used a four step extraction procedure followed by pyrolysis gas chromatography−mass spectrometry (Py-GC/MS) to quantify PS and PMMA nanoparticles in cucumber plants after hydroponic exposure(Li et al., 2021). The variety of individual plant responses observed in previous studies in terms of growth, chlorophyll contents and/or oxidative stress (Larue et al., 2021; Wu et al., 2021; Yin et al., 2021) points out the need to develop new experimental approaches to allow for the tracing of this analytically challenging target material and to provide a basis of interpretation of the reported effects.

This study aimed at evaluating the uptake and impacts of nanoplastics on wheat (*Triticum aestivium L.*), a model plant and staple food source, and at providing a proof of concept of a new combination of approaches including classical phytotoxicity markers and advanced imaging and nanometrology techniques. We have used polystyrene (PS) nanoparticles doped with Pd. In order to specifically study the effects of particle morphology on plant response, two different

nanoplastics morphologies have been used, so called smooth (S) and raspberry (R). These nanoplastics present a core-shell structure with a core of Polyacrylonitrile (PAN) containing the metal tracer and a shell of cross-linked PS (Mitrano et al., 2019). The stability of these nanoplastics and their utility to study the fate of nanoplastics in complex organic matrix such as sewage sludge or animal models has been demonstrated in previous studies (Clark et al., 2022; Frehland et al., 2020; Keller et al., 2020; Lahive et al., 2022; Redondo-Hasselerharm et al., 2021). Polystyrene (PS) is one of the most commonly produced commodity seven polymers(Geyer et al., 2017). Its detection in organic fertilizers and compost(Brinton, 2005; Weithmann et al., 2018) as well as in soils (Chen et al., 2020; Fakour et al., 2021; Fuller and Gautam, 2016; Piehl et al., 2018; Scheurer and Bigalke, 2018) suggests that it may be broadly present in agricultural soils.

The use of metal-doped nanoplastics expanded our analytical possibilities to techniques normally reserved for metal analysis, such as synchrotron micro X-ray Fluorescence (μXRF) and inductively coupled plasma mass spectrometry (ICP-MS). μXRF has been demonstrated to be a unique technique to study the interaction of plants with engineering nanomaterials (ENMs), it provides multi-elemental detection with lateral resolution providing important information to understand uptake, transport and storage mechanisms(Castillo-Michel et al., 2017). Combining this with Fourier transformed infrared spectroscopy (FTIR), micro and nano computed X-ray tomography (μCT and nanoCT) and scanning electron microscopy (SEM), we could additionally assess effects on root architecture and particle-root interaction. FTIR provides insights on the cell wall composition and possible shifts of some families of molecules (Canteri et al., 2019), with the appropriate chemometric analysis, it is an ideal technique for the screening of plant response against stress when previous knowledge is scarce and/or contradictory, as it is the case for micro and nano plastic exposed plants. X-ray computed tomography allows for the 3D reconstruction of scanned objects, it is non-destructive and requires minimal sample preparation avoiding the production of surface artefacts. It has been extensively used in the study of plant root traits (Dhondt, 2012; Gao et al., 2019). In the present study, we used μCT to assess possible impacts of the nanoplastics on root structure and nanoCT to search for nanoplastics in the root tissues. Although FTIR has been successfully applied to investigate the interaction of nanomaterials with different plant tissues (Bakshi et al., 2019; Liné et al., 2021; Savassa et al., 2021) and lab bench μCT has been used for the visualization of ENMs in plant roots (Avellan et al., 2017; Pradas del Real et al., 2017b), to our knowledge, this is the first time that FTIR and synchrotron μ and nanoCT are used together to study the effects of nanoplastics on plant root structure. Besides, thanks to the high flux and coherence of synchrotron source, synchrotron based CT provides images with higher quality than lab-bench CT and allows the detection of phase contrast which is about 2 orders of magnitude more sensitive than absorption contrast (obtained in lab CT scanners). This information is of high relevance since plant roots are the first barrier of the plant to be in contact with nanoplastics, they regulate nutrient and water uptake by plants and they are drivers of many ecological functions (Freschet et al., 2021). Using an integrative approach, we not only assess classical phytotoxicity markers for plant growth and quality, but developed analytical tools to assess effects on cell walls (with FTIR-ATR, μCT, nanoCT and SEM) as well as use metal-doped nanoplastic particles to more clearly assess interactions, uptake and transport (with μXRF and ICP-MS). In particular, we aimed to 1) quantify the uptake on nanoplastic and localize the main transport and accumulation in tissues, 2) study the influence on physiological development (biomacromolecule composition, root morphology and root exudation), and 3) provide further development of powerful analytical tools which can help to facilitate more detailed and careful research into the interaction of nanoplastics with plants in the future.

2. Methods

2.1. Pd-doped nanoplastics

Emulsion polymerization of inorganic metal-doped nanoplastics spheres were made in house (Mitrano et al., 2019). Briefly, the procedure consisted of a two-step process in which first the particle core was synthesized (which contained the metal), after which a further shell of polystyrene was grown through feeding a second monomer-containing solution over time to augment the surface chemistry and morphology of the original particle. For the nanoplastics core, a surfactant (SDS) and initiator were charged inside the reactor. When the initial nucleation point was achieved, the dissolved metal precursor was added slowly to the reaction vessel. The evolution of the polymer conversion and particle size were followed through dynamic light scattering (DLS) (Malvern Zetasizer Nano Z, backscatter angle 173o at 25 ^{o}C) and thermogravimetric analysis (TGA) at T=120 oC (Mettler Toledo), respectively. After a conversion rate of approximately 90% was achieved, the shell feed was directly plumbed into the reaction vessel along with an additional shot of initiator and water. The shell feed, a mixture of water, styrene, DVB and SDS, was dosed for four hours. Two distinct shell morphologies were used in this work; so called smooth (S) and raspberry (R), with average diameters of approximately 160 nm (supplementary figure 1). Using these two different metal-doped nanoplastics allowed us to specifically isolate and study the potential impacts of particle morphology, since the other particle characteristics (e.g. agglomeration state, surface charge, chemical composition) were similar. The total Pd content was approximately 0.5% for both types. The concentration of nanoplastics in the stock solutions were between $6.22 \cdot 10^{16}$ to $8.88 \cdot 10^{16}$ particles$\cdot$mL^{-1}.

2.2. Assessment of Pd stability in nanoplastics

Stability of the Pd tracer inside the nanoplastics is paramount throughout the experiments as we rely on the Pd signal to assess nanoplastics uptake and localization. To assess the possibility of Pd leaching over time inside the plant, we simulated the conditions inside the plant cell environment by exposing the nanoplastics (corresponding to 1 mg Pd$\cdot$L^{-1}) to a nutrient solution (10 mL) containing KNO_3 (150 mM), $NH_4H_2PO_4$ (50 mM), $MgSO_4$-$7H_2O$ (0.5 mM), $Ca(NO_3)_2$-$4H_2O$ (100 mM and NaCl (5 mM), oxalic acid (5 mg$\cdot$L^{-1}), glucose (10 mg$\cdot$L^{-1}) and BSA (2.5 mg$\cdot$L^{-1}) initially adjusted to pH 5, in an end-over-end shaker for three weeks. To simulate ROS production in the plant, which had the potential to induce further Pd leaching, twice weekly spiked additions of H_2O_2 at low/realistic (7 mM) and high/extreme (70 mM) were made throughout the experiment. Nanoplastics suspensions, without the addition of salts or H_2O_2 in DI H_2O, were used as a control. Triplicate samples were sacrificed at weekly time intervals (i.e. 0, 1, 2, and 3 weeks) and passed through an centrifugal ultrafilter (10 kDa pore size) and filtrate was analyzed by ICP-MS to assess Pd leached from the nanoplastics over time. The quantification limit of Pd by ICP-MS was 10 ng$\cdot$L^{-1}.

2.3. Plant culture

Seeds of wheat plants were sterilized on 70% ethanol (v/v) for 5 min, rinsed with distilled water, and germinated in moisture vermiculite at 24°C under dark conditions. Once the cotyledon was developed (5 days), seedlings were transferred to a hydroponic system and allowed to acclimate for one week in 1/4 strength Hoagland nutrient solution: (0.75 mM KNO_3, 0.25 mM $NH_4H_2PO_4$, 0.13 mM $MgSO_4.7H_2O$, 0.5 mM $Ca(NO_3)_2.4H_2O$, 12.5 µM NaCl, 6.25 µM H_3BO_3, 0.5 µM $ZnSO_4.7H_2O$, 0.5 µM $MnSO_4 \cdot H_2O$, 0.03 µM $CuSO_4 \cdot 5H_2O$, 0.13 µM $(NH_4)6Mo_7O_{24} \cdot 4H_2O$, 5 µM Fe(III)-EDTA), pH = 5.7. Wheat plants were exposed to the following treatments added to the nutrient solution: i) 3 mg$\cdot$L^{-1} raspberry nanoplastics (3R) ; ii) 30 mg$\cdot$L^{-1} raspberry nanoplastics (30R); iii) 3 mg$\cdot$L^{-1} smooth nanoplastics (3S); iv) 30 mg$\cdot$L^{-1} smooth nanoplastics (30S)and v) no

plastic addition (C). The nanoplastics suspension used to spike the nutrient solutions could potentially contain some surfactants and residues from the synthesis process. In order to ensure that observed effects were only due to the nanoplastics and not to any of these surfactants and/or residues, we performed and additional control (CSN). To this end, the 30 mg·L^{-1} raspberry nanoplastics suspension was filtrated to remove the nanoplastics and the filtrate was used to spiked the nutrient solution. The hydroponic system consisted on 24 polypropylene pots containing 0.7 L of the nutrient solution. Ten plants per pot were placed in floating polystyrene (PS) disks of 15 cm diameter. The release of particles from these PS disks ($5.38 \cdot 10^8$ particles per disk based on the determinations of Lambert et al. (2016) (2016)) was negligible compared to the number of particles in the spiked solutions (between $5.22 \cdot 10^{15}$ and $7.45 \cdot 10^{17}$ in the 3 mg·L^{-1} treatment and between $5.22 \cdot 10^{16}$ and $7.45 \cdot 10^{18}$ in the 30 mg·L^{-1} treatment). Our choice of these concentrations was mainly analytical – we aimed to have a plastic concentration where we would be confident that we could measure the metal tracer above analytical detection limits. However, it is worth noting that previous studies which have attempted to detect nanoplastics in plants (not seedlings) used doses between 10 and 55 mg·L^{-1} (Li et al., 2021; Lian et al., 2020; Sun et al., 2020; Zhang et al. 2019a). Therefore, the dose of 30 mg·L^{-1} used in the present study falls within the range which has already been used in literature, and we were able to even decrease this exposure concentration by 10 times (i.e. to 3 mg·L^{-1}), which further shows the advantage of using metal-doped plastics, ICP-MS, and the microscopy techniques used here.

The system was continuously aerated and kept under controlled conditions (day/night photoperiod 12/12h, 20/18°C, 70/60% humidity, 200/0 µmol m^{-2} s^{-1} light intensity).

Plants were randomly selected to be exposed to 3 or 30 mg nanoplastics L^{-1}, either smooth (S) or raspberry (R). Nutrient solution without nanoplastics was used as a control. An additional control was prepared to identify the potential effects of the solution in which the nanoplastics were suspended, which may have contained trace concentrations of surfactant or unpolymerized monomer from the synthesis process. The raspberry nanoplastics suspension was centrifuged for 40 min at 60200 g to settle all nanoparticles into a pellet, then the supernatant was decanted and added to the nutrient solution in the same volume as in the 30 mg L^{-1} nanoplastics treatments. Four independent replicates were used for each treatment (n=4).

A separate plant culture experiment was performed in similar conditions to prepare additional samples for micro X-Ray fluorescence (µXRF) mapping. In this case, plants were grown in glass pots containing 0.5 L of nutrient solutions.

2.4. Analyses of the nutrient solution

At each renewal of the nutrient solution, three parameters were measured in both the fresh solution and in the solution after 3 or 4 days of contact with the plants (i.e. aged solution). The hydrodynamic diameter and zeta potential of the nanoplastics were measured using a nano zeta sizer (nanoZS, Malvern) for the 30 mg L^{-1} dose only because the 3 mg L^{-1} dose was below the detection limit. The pH of the solutions was measured for all conditions at each time point. The concentrations in total organic carbon (TOC) and low weight organic acids (LWOAs) were determined on the last aged solution at the time of harvesting. TOC was measured with a TOC-VCSN analyzer (Shimadzu). For LWOAs, an aliquot of 50 ml from each pot was frozen in liquid N_2 and freeze-dried. The freeze dried samples were re-suspended in 0.4 mM of heptafluorobutiric acid and filtered at 0.20 µm. Then LWOAs were determined by ionic chromatography (Dionex DX 500) using a conductivity detector. Chromatogram conditions are described in Pradas del Real et al. (2017a).

2.5. Harvesting and sample conditioning

After three weeks of exposure, wheat plants were harvested, and their shoots and roots were immediately separated at the root-shoot junction. Both roots and shoots were washed with distilled water and weighed to determine fresh biomass. From each pot, different plant aliquots were prepared for subsequent analyses. For the determination of physiological parameters, subsamples were immediately frozen in liquid N_2 and stored at -80ºC until analysis. For the determination of dry mass, ICP-MS analyses and Fourier transform Infrared spectroscopy (FTIR), subsamples were dried in an oven at 70 ºC for 48 h and stored in a desiccator until analysis.

The roots tips and elongation zone of five roots per condition were prepared for analysis by scanning electron microsocopy (SEM) and synchrotron-based computed microtomography (µCT). Samples were immediately fixed in 2.5% glutaraldehyde in 0.1M sodium phosphate buffer (pH 7.2) and left overnight. Then they were washed (3 times, 10 min per wash) with 0.1 M sodium phosphate buffer (pH 7.2) followed by serial transfer in ethanol series: 30%, 50%, 70%, 80%, 90%, 95%, 100% (2 times, 10 min duration). Samples were then subjected to critical point drying (CPD) using a Leica EM CPD300 instrument.

For µXRF analyses, root samples were separated from shoots and thoroughly washed after harvest. The apexes were sectioned, frozen in isopenthane, cooled in liquid N_2 and immediately freeze dried at -50ºC and $1{\cdot}10^{-2}$mbar in an Emitech 750 freeze drier. Mature zone of the roots were embedded in Optimal Cutting Temperature (OCT) resin (Leica), frozen in isopenthane and cross-sectioned (20µm) using a cryomicrotome (RM2265/LN22 Leica).

2.6. Nanoplastics concentration in plant tissues

Pd content in plant biomass was determined by induced coupled plasma mass spectrometry (ICP-MS) after microwave assisted acid digestion. Approximately 100 mg of sample was placed into a Teflon digestion tube, 1 ml H_2O_2 (30%, Sigma-Aldrich, USA) was added. After 1 h, 4 ml of HNO_3 was added (in two separate aliquots of 2 ml each) and allowed to stand for an additional hour. Finally, 0.5 ml of H_2SO_4 (Rotipuran® Supra 95 %, Carl Roth, Germany) was added. Samples were subjected to 253°C at 100 bar over 25 min in a microwave digester (Ultraclave, MLS GmbH, Germany). Pd concentrations were measured by ICP-MS (8900 ICP-MS Triple Quad, Agilent Technologies, US) and Indium was used as internal standard. Calibration solutions ranging from 0.1 - 50 $\mu g{\cdot}L^{-1}$ were produced from Pd standard solutions (Palladium standard for ICP 10,000 $mg{\cdot}L^{-1}$, Sigma-Aldrich, US) in 2 % nitric acid (Rotipuran® Supra 69 %, Carl Roth, Germany). Pd concentrations in samples were converted into nanoplastics (mass) concentrations based on their average Pd content of 0.5%.

Based on calculated nanoplastics concentration in shoots and roots, the transfer factors (TF) were determined as described in Supplementary Information.

2.7. Nanoplastics distribution in roots

After critical point drying, roots were coated with carbon and imaged by SEM with a FEG ZEISS Gemini SEM 500, coupled with an energy dispersive X-ray analyzer (EDX, EDAX OCTANE ELITE 25) at 3 to 10 kV in high vacuum mode. The region examined was located at 400 µm from the root tip. One to two roots per condition were analysed.

Freeze-dried root tips and fresh cross sections from the mature zone were studied by synchrotron micro X-Ray fluorescence (µXRF) on the scanning X-ray microscope at ID21 beamline of the ESRF (The European Synchrotron Radiation Facility, Grenoble, France). Focusing was done using a Kirkpatrick–Baez mirror system ($0.7x0.5\mu m^2$). Fluorescence mapping was done

at 7.2 keVs for root apex and at 5.1 keVs for cross sections with dwell time of 100 ms. For root cross sections, measurements were performed in cryogenic conditions using a vibration-free cryo stage, passively cooled by a liquid nitrogen Dewar. In both cases, emitted fluorescence was recorded on a silicon drift detector (SGX Sensortech 80 mm^2 active area) and drilled photodiode was used as incoming intensity monitor. Elemental maps presented in this article were obtained by fitting each pixel fluoresce spectrum using PyMCA (Solé et al., 2007) software as described in Castillo-Michel et al. (2017). Images from the control processed by the fitting routine presented a background signal in the Pd channels. In order to subtract this background from all control and nanoplastics treated samples, filter masks were produced for epidermis and cortex/vascular regions. From the average XRF spectrum of the control map the Pd fit area did not satisfy the criteria of instrument limit of detection (LOD) defined as fit area≥3* standard deviation. For treated maps the epidermis and cortex-vascular region masks were used to produce average XRF spectra and the LOD criterion was satisfied only for the epidermis region. The maps in figure 1c present the Pd signal obtained from applying the filtering masks at the epidermis, the XRF average spectra resulting from this analysis and the corresponding fitting areas and sigma values are shown in supplementary figures 7 and 8.

The root samples prepared by critical point drying were mounted on top of quartz capillary to be imaged using synchrotron-computed nanotomography at ID16B nano-analysis beamline at the ESRF. Here a holotomography technique was used: four tomographies were acquired using a beam energy of 29.5 keV and a flux of $1.5x10^{11}$ ph/s. For each tomography, 3203 phase contrast images with a pixel size of 25 nm were recorded over 360°using a PCO edge 5.5 camera. The acquisition time per 2D projection was 30ms. The phase retrieval was performed using a contrast transfer function approach (CTF) (Cloetens et al., 1999). The 3D volumes were reconstructed via filtered back projection using the PyHST2 software at the ESRF (Mirone et al., 2014). Segmentation was performed using Avizo (version 2019.3, Thermo Fischer Scientific Inc., Massachusetts) and Matlab (version 9.5.0 (R2018b), The MathWorks Inc., Massachusetts).

2.8. Phytotoxicity markers

The level of lipid peroxidation was determined in terms of malondialdehyde (MDA) content according to Health and Packer (1968) modified for these samples (Heath and Packer, 1968). Photosynthetic pigments were analysed as described in Larue et al. (2014) (2014). The protein content was determined according to Bradford method (1976) using bovine serum albumin (BSA) as standard (Bradford, 1976). Further description of these method is provided in Supplementary Information.

2.9. Biochemical composition

The effect of nanoplastics exposure on the biochemical composition of plant tissues was studied by Fourier Transform Infrared Spectroscopy in Attenuated Total Reflectance mode (FTIR-ATR) on freeze dried powdered samples. Samples were analysed using a FTIR spectrometer with an ATR accessory (Thermo Nicolet NEXUS 470 ESR) over the range of 4000 – 400 cm^{-1} with a spectral resolution of 4 cm^{-1}. One spectrum was the average of 64 scans per sample. Four biological replicates per treatment were collected, with four technical replicates performed for each biological sample.

2.10. Impact on root structure

Roots prepared by critical point drying were mounted into small plastic vials and subjected to synchrotron-computed microtomography in ID19 beamline at the ESRF. Scans were acquired at 26.5 keV, close to Pd K-edge (24.3 keV). In total 4000 projections were acquired with a pixel size of 0.72 µm and an acquisition time of 50 ms each over a rotation of 360°. Several scans along

the z axis were performed and merged in order to cover a sufficient field of view. Reconstruction was done by exploiting the phase contrast using the Paganin´s method applying a delta/beta ratio of 300, coupled to conventional filtered back projection. The reconstructed 3D image made of voxels corresponds to a map of the refractive indices stored in units of $2\pi/\lambda$, with λ being the wavelength of the X-ray beam. This map is linearly related to mass density. The reconstructed values are converted to 16bit integer values and referred to as gray values

For each sample, a region of interest was chosen within the elongation zone, such as to maximize the analysed volume but neglecting regions with damaged tissue. The segmentation of the plant cell walls and air, as well as the segmentation into different structural regions (epidermis, cortex and stele) was achieved by an iterative approach combining Avizo (version 2019.3, Thermo Fischer Scientific Inc., Massachusetts,) and Matlab (version 9.5.0 (R2018b), The MathWorks Inc., Massachusetts).

In a first step, a rough watershed algorithm was used to segment the cells from the surrounding air. To separate cells that might have a connection after the rough watershed segmentation, a 'separate objects' step was performed on the 3D data. On a slice-wise basis, the cell area was determined such that the structural regions (epidermis, cortex and stele) could be assigned according to the cell size. By combining multiple morphological operations, masks for each region were created. These masks were multiplied with the original respective gray value volumes and a second watershed algorithm performed within a) the stele and b) within the epidermis and cortex. These results were finally combined and cleaned with a 'separate objects' step on the 3D data. This process resulted in masks for the segmented cell walls, the cells, and the different regions of interest (i.e. epidermis, cortex and stele).

The areas and number of the segmented cells were analysed along the root length for the epidermis, the cortex and the stele. For these cells, their volumes were also determined individually for each of the three regions. The masks of the cell walls were used to determine the local cell wall density in 3D. Based on averaged gray values along 20 µm from the root middle region, three thresholds were established (high, medium and low) and used to produce masks of cell wall density regimes. Subsequently, the number of pixels from each mask were extracted to show the percent of pixels from each regime in each sample. Figure 16 in Supplementary information shows the thresholding method. Since all samples were imaged and reconstructed in the same way, the gray values (as a measure of the mass density) were compared between the different tissue regions and samples. Figure 4 illustrates the different steps of this segmentation process.

2.11. Statistical analyses

Statistical analyses were performed using the SPSS software. Normality and homogeneity of variances were tested by Shapiro-Wilk and Levene's tests, respectively. The analysis of variance for variables with homogeneous variances, was performed by one-way ANOVA followed by a post-hoc Tukey's (HSD) test at the 5 % level. The variables with non-homogeneous variances were analysed using Welch method followed by Dunett post hoc test.

Pre-processed FTIR spectra were analysed using Orange Data Mining software (Demšar et al., 2013). Linear Discriminant Analysis (LDA) together with Principal Component Analysis (PCA) was applied to cluster the samples. Logistic Regression with Least Absolute Shrinkage as Selection Operator (LASSO) was used to identify the main features contributing to differences between treatments. The robustness of the model was monitored using a K-fold cross validation method. The model's robustness parameters AUC (Area Under Curve), receiver operating characteristic

(ROC) curve, precision, and sensitivity (or recall) were reported. Boxplots of cell volumes were performed using Pandas package in Phyton.

3. Results and discussion

3.1. Nanoplastics are absorbed by roots and transported to the shoots

Thanks to the use of Pd-doped nanoplastics, the present study provides quantitative information about the uptake and transfer to the shoots of nanoplastics by a plant. In order to test the stability of Pd in the nanoplastics, a leaching experiment was performed in DI H_2O and in simulated plant cell environment with low or high H_2O_2 pulse additions over three weeks. While a very small proportion of Pd was not incorporated into the nanoplastics upon initial synthesis (0.5%), no further Pd release was measured over the duration of the experiment. In all tested conditions, the concentration of free Pd was lower than 0.05% (Supplementary figure 2). Therefore, Pd can be used as a proxy to calculate nanoplastics concentration in plant tissues but the plant is not exposed to Pd itself, which is securely encapsulated within the plastic. Pd was detected both in the plant roots and in shoots, meaning that nanoplastics were absorbed by plant roots and translocated to the shoots (figure 1a). The total concentration of nanoplastics in plant tissues was dose-dependent, however no significant differences were found between different nanoplastics surface morphologies (smooth surface vs. rough surface so called raspberry), where particle size and surface chemistry were otherwise similar (supplementary figure 1 and 4). Transfer factors were significantly higher ($p<0.05$) in 3 $mg \cdot L^{-1}$ treatments than in the 30 $mg \cdot L^{-1}$. This may be related to the presence of larger agglomerates on the root surface in the high dose treatment, which may limit the internalization and transfer of the individual nanoplastics.

Agglomerates of nanoplastics were observed at the surface of roots exposed to both 3 and 30 $mg \cdot L^{-1}$nanoplastic (figure 2 and Supplementary figure 3). Nanoplastics were associated to a network of filaments on the root surface. These structures may belong to the root cap mucilage (Tran et al., 2016) but they can also be produced by bacteria developed on the surface of the roots (Gantar et al., 1995). Bacteria were observed on the root surface in all conditions (figure 2 and Supplementary figure 3). They may correspond to the various species previously identified in the rhizosphere of wheat (Matos et al., 2005), although no identification was performed in this study. In a recent study, Li et al. (2020) suggested that the entrapment of PS beads in the root mucilage of wheat and lettuce promoted their adhesion on the root surface (Li et al., 2020). Inorganic engineered nanoparticles (ENPs) differ in many aspects from nanoplastics. However, at least those which are resistant to dissolution, such as TiO_2 and AuNPs, share some physico-chemical properties and potential transformations (e.g., homo and hetero aggregation, changes in surface charge, formation of an 'ecocorona') with nanoplastics (Syberg et al., 2015). Therefore, some prior knowledge on ENPs behaviour in this system can be used to put our results into perspective. The agglomeration of ENPs with root mucilage has been reported in a wide variety of terrestrial plants and, in general, it has been related with a decrease in the uptake and translocation to the shoots, with the exception of positively charged and/or small (i.e. < 20 nm) ENPs (Schwab et al., 2016).

After 3 - 4 days of culture, an increase in the average particle hydrodynamic diameter was observed for the nanoplastics of the 30S and 30R treatments that was accompanied by a

decrease of their surface charge (Supplementary figure 4). These analysis of the nutrient solution confirmed the agglomeration of nanoplastics during plant growth, due to the combined effects of high ionic strength, root exudates and other rhizodeposits, and increased pH (more details in Supplementary Information). Root exudates play a key role in plant nutrient acquisition. Changes in the concentration of these compounds may provide some insights on the impact of the presence of nanoplastics in the plant, as shown for plants exposed to metallic and organic contaminants(Chaudhry et al., 2005; Dong et al., 2007). A recent study on a dicot showed an increase in the exudation of oxalate in *Arabidopsis thaliana* exposed to PS nanoplastics(2020). In the present study, the concentration of low weight organic acids (LWOAs) was determined at the end of the culture. Different changes in concentration were found depending on the of organic acids analysed (Supplementary figure 5). A significant increase ($p<0.05$) was found for the 3S treatment in the case of citric, malic, lactic and succinic acids and for the 30S treatment in the case of oxalic acid. The concentrations of formic and acetic were not affected by nanoplastics treatments. PCA-LDA performed on the organic acid concentration data (supplementary figure 5b) show that their composition varied as a function of the type of nanoplastics and dose, as shown by In addition, an increase in total organic carbon was found in the nutrient solution of plants exposed to nanoplastics compared to controls (supplementary figure 5a). These results are evidence of a complex response from the plant to nanoplastics, affecting different classes of rhizodeposits.

The localization of the nanoplastics was studied by µXRF, using the Pd signal, on entire root tips (Figure 1b) and on root cryo-sections from the maturation zone (Figure 1b) of plants exposed to 30 $mg \cdot L^{-1}$ nanoplastics. Nanoplastics were detected in the root cap and on the epidermis of root maturation zone in association with the cell wall (Figure 1), but not in the cortex or in the vascular cylinder (Supplementary figures 7 and 8). Previous studies have shown an accumulation of nanoplastics at the surface of the root cap of *Vicia fava, T. aestivum, Arabidopsis thaliana* and *Oryza sativa* with or without evidence of internalization (Jiang et al., 2019; Lian et al., 2020; Liu et al., 2022; Sun et al., 2020; Taylor et al., 2020). The µXRF results, combined with the evidence of nanoplastics uptake and translocation, suggest that the root cap is a point of entry of nanoplastics in wheat plants. A similar finding was presented for some ENPs into the plants. The loose of junctions between cells in this location offer a pathway for small particles entry (Schwab et al., 2016).

3.2. Impacts on root architecture despite low phytotoxicity

The exposure to nanoplastics did not induce negative effects on plant development in terms of total biomass, oxidative stress or chlorophyll and protein contents (supplementary figures 9-12). The absence of significant impacts on broad phytotoxicity parameters found in wheat plants is in accordance with previous studies, showing no significant effects for *A. cepa* and *V. faba* exposed to doses < 100 $mg \cdot L^{-1}$ (Giorgetti et al., 2020; Jiang et al., 2019). Conversely, Lian et al., (2020) found positive but non-monotonic responses for *T. aestivium*(Lian et al., 2020). On the other hand, Li et al. (2020) found different effects in *Cucumis sativus* exposed to 50 $mg \cdot L^{-1}$ of PS nanoparticles depending on the size of nanoparticle and the parameter studied. Sun et al. (2020) found different responses depending on the surface charge of the nanoplastics. Collectively, this suggests that the ability of plants to modulate antioxidant levels and the expression of genes related with oxidative stress in order to neutralize the effects of ROS production (Sun et al., 2020) strongly depends on the specie investigated, the characteristics of the nanoplastics and the dose. This also highlights the need to develop new approaches to measure other phytotoxicity endpoints. As indicated in the previously mentioned studies, metabolic, cytologic

and genotoxic alterations may all be possible. Therefore, we developed a methodology to screen for potential biochemical alterations caused in wheat tissues because of nanoplastics exposure based on the use of ATR-FTIR together with a robust multivariate analysis.

PCA-LDA performed on ATR-FTIR spectra from roots and shoots showed clear clustering of treatments (figure 3). The main FTIR bands explaining the differences among treatments were selected by Logistic regression with a LASSO estimator are provided in the supplementary material (Supplementary table 1). An increase in the absorbance of different bands related with carbohydrates and cell wall components (cellulose, pectin and lignin) was found for 30 $mg{\cdot}L^{-1}$ treatments and 3 $mg{\cdot}L^{-1}$ smooth treatment in roots, which is indicative of a reinforcement of the cell walls. Conversely, a decrease of these bands was observed in the shoots, suggesting weaker cell walls. Additionally, in both roots and shoots, spectral variations were observed for IR bands related to amides, which indicates that the protein pool was affected as well.

Synchrotron µCT was used to further study the impacts of nanoplastics on root cell walls and architecture (figure 4). Results confirmed the reinforcement of the cell walls in roots from the 30 $mg{\cdot}L^{-1}$ smooth treatment. An increase in the proportion of voxels in the medium and high-density regime was observed for this treatment in comparison to the control (Figure 5a and b). This increase in cell wall density was mainly located in the epidermis of exposed roots, with some significant spots located in the endodermis, likely corresponding to the Casparian strip (Fig 5 a and b). Approximating the roots to cylinders (figure 4 a), the small differences in surface to volume ratios among samples cannot account for the differences observed in the proportion of density regions. A decrease in the volumes of epidermal cells was also observed in roots from this treatment (Figure 5 c). 3D reconstructions of the analysed roots are provided in Supplementary material. The 3D rendering of the gray values using a temperature color bar clearly shows the higher proportion of voxels in the high-density regime in the surface of treated roots, especially for the 30 $mg{\cdot}L^{-1}$ smooth treatment. The adapted contrast images highlight that this increase is found not only on the surface but also throughout the entire epidermal layer, which is subsequently translated into a decreased cellular volume.

The reinforcement of the cell wall is a well-known response to biotic and abiotic stress developed by plants to preserve cell wall integrity and cell turgor (Le Gall et al., 2015). Furthermore, the adsorption of pollutants to the cell wall is widely described as a detoxification mechanism in plants to reduce their presence in the cytoplasm, interference with cell functioning (Krzesłowska, 2011), as well as to regulate transport through plant tissues (Song et al., 2013). For example, some plant species exposed to divalent and trivalent metal ions increase the biosynthesis of cell wall compounds to increase the trapping capability of the cell wall (Krzesłowska, 2011). Fine µXRF analysis showed the presence of nanoplastics within epidermal cell wall (Figure 1c), so a similar mechanism is plausible in this study as well. However, the reinforcement of root cell walls as a response to nanoplastics exposure seems to have a negative impact to the cell walls of shoots, where a decrease in the absorption bands of the same components can be indicative of the weakening of these structures. On the other hand, the decrease in the cell volumes of the epidermis of roots exposed to 30 $mg{\cdot}\ L^{-1}$ smooth nanoplastics may be another consequence of the cell wall reinforcement as cell walls are responsible for the mechanical control of cell size and shape (Le Gall et al., 2015). Collectively, these results suggest that smooth nanoplastics have a more pronounced impact on cell wall composition and root structure than raspberry nanoplastics. Although the raspberry nanoplastics had a bumpier surface, the two types of nanoplastics had similar zeta potentials and sizes (Supplementary Figure 4). So, with the available data, it was not possible to explain the difference found in the

plant response against the two nanoplastics morphologies. Further investigations on other physico-chemical parameters of the plastics properties which most influence uptake would be necessary for further interpretation, which suggests that future studies should consider to use an array of particle sizes, shapes and surface characteristics to understand the varied stress responses of plants to plastics.

Alterations in the protein pool were also detected in both roots and shoots. Cross linked structural proteins play an important role in the regulation of cell wall plasticity (Le Gall et al., 2015), however, it is not possible to confirm if the observed changes are also related with the cell wall conformation or with any of the other critical functions played by proteins in plant cells. Alterations in carbohydrate and aminoacid metabolism have been recently reported in wheat plants exposed to PS nanoplastics (Lian et al., 2020), so it is also plausible that the biochemical changes observed here are the consequence of alterations in basic metabolic pathways. On the other hand, some studies have shown a relationship between cell wall reinforcement and changes in root exudation in plants under stress, (Feng et al., 2020) especially due to pathogen infection (Brahmi et al., 2016; Castilleux et al., 2018; Vandana et al., 2019). If such a relationship between the changes in biochemical composition of plant tissues and root exudation in wheat exposed to nanoplastics exists remains to be elucidated. However, an increase in total organic carbon in the nutrient solution due to the passive loss (senescence or turnover) of reinforced cell walls in exposed plants cannot be excluded (de la Fuente Cantó et al., 2020).

3.3. Advances in nanometrology to assess nanoplastics interactions with plants

The carbonaceous nature of plastic makes its detection in organic matrices, such as plant tissues, a challenge which is exacerbated in the case of nanoplastics due to their small size. This is one of the reasons for the scarce number of studies regarding nanoplastics-plants interactions. Recent studies using fluorescent-labelled PS nanoplastics have provided evidence of their internalization by different plant species (Chae and An, 2020; Giorgetti et al., 2020; Jiang et al., 2019; Li et al., 2020; Lian et al., 2020; Liu et al., 2022; Sun et al., 2020). However, the use of fluorescent-labelled nanoplastics is limited to direct observation under a microscope and suffers from artefacts such as fluorophore leaching and tissue autofluorescence. This approach also fails to provide quantitative information about the uptake and distribution to different plant tissues. The present study demonstrates that the use of Pd-doped nanoplastics is an excellent approach to overcome these pitfalls as it allows the use of techniques such as synchrotron µXRF and ICP-MS. On one hand, the better detection limits of these techniques compared to that of microscopic techniques previously used allowed us to detect nanoplastics in wheat plants at lower and probably more realistic doses (3 $mg \cdot L^{-1}$ vs. 10-100 $mg \cdot L^{-1}$). ICP-MS and XRF techniques overcome the issue of matrix complexity by using a non-endogenous metal incorporation (Pd) as the proxy for their fate in plant tissues. The detection of Pd by ICP-MS allowed us to quantify the uptake of nanoplastics as a function of their concentration in the nutrient solution as well as the relative transfer to the shoots, where they are found at much lower concentrations, which has not been previously accessible by microscopic techniques. Taking further advantage of the Pd labelling of the nanoplastics, the use of synchroton µXRF allowed us to identify the root cap and the maturation zone of roots as the main points of accumulation and potential absorption of nanoplastics in roots, while preserving the close to native environment thanks to cryogenic conditions. It also allowed us to show the accumulation of nanoplastics within epidermal cell walls. The spatial resolution of synchrotron XRF is given by the beam size, and current technology allows one to focus the X-ray beam down to the nanoscale (~25nm). In this work the

resolution was 1µm. Other points of entry described for ENPs, such us root hairs or cracks at sites of lateral root emergences, may also be applicable for nanoplastics as well. For example, Li et al. (2020) suggested that the later could be a major point of entry for microplastics in wheat and lettuce(Li et al., 2020). The broad resolution range of synchroton XRF may allow to select the adequate set-up to investigate these additional uptake mechanisms for Pd-doped nanoplastics as well as their transport (symplastic vs apoplastic) in plant tissues. Quantification of nanoplastics in plant tissues using Py-GC/MS is a promising technique recently tested and shows good detection limit(Li et al., 2021). However, the advantage of using of Pd doped nanoplastics over this approach is the possibility to have both quantitative and imaging information over the same set of samples, which is an asset to study uptake and transport mechanisms.

The innovative combination of ATR-FTIR with synchrotron µCT has shown the primary role of the cell walls in the response of wheat plants to nanoplastics exposure. Whether this is a regulated response to control the damage produced by nanoplastics or a consequence of metabolic impairments remains to be elucidated. Of note is the high correlation between nanoplastics distribution shown by µXRF and the increase in density observed in the epidermis by µCT. With the available data, it is not possible to conclude if nanoplastics accumulation has contributed to increase gray value distribution (which is scaled with the mass density) in this tissue region. However, taking into account the small size of nanoplastics regarding voxel size, the potential contribution to phase contrast would be minimal in comparison to the one caused by morphological alterations of the tissue. A control root and a root exposed to 30 $mg \cdot L^{-1}$ smooth nanoplastics were investigated by synchrotron computed nanotomography (nanoCT). Thanks to a pixel size of 25nm this technique provides a more detailed view of cellular structures than µCT and should allow the visualization of nanoplastics (160 nm). However, as it is shown in figure 6 and supplementary figure 18, globular structures with sizes below 1 µm that can correspond to nanoplastics and/or small nanoplastics aggregates were identified both in the control and the treated roots. They were mainly located close to the cell walls of cortex cells. Indeed, plant cells contain various components which may appear similar to nanoparticles (e.g., polyphosphate granules, small vesicles, etc). While we were not successful in the detection of nanoplastics using nanoCT, we must emphasize that this technique is still promising to eventually detect nanoplastics in complex matrices with further analytical method development. Furthermore, these results bring into question the validity of some of the previously published data regarding the detection of nanoplastics in plant tissues using transmission electron microscopy (TEM). One has to take into account that the use of nanoCT allows scanning over a wide area and the ability to reconstruct multiple sections. This is in contrast to analyzing samples with TEM where only a few thin sections or micrographs are analysed so the probability of having a nanoplastic in any given thin section would be low and the probability of (incorrectly) identifying a structure as a nanoplastic when it is in fact a naturally occurring feature is high. For example, in two recently published manuscripts, the authors speculated that they identified nanoplastics in plant tissues based on TEM images alone.(Dong et al., 2021; Lian et al., 2021) This result is highly questionable since no control TEM images of the plant tissues are shown and therefore there is no clear evidence that the globular structures the authors identified correspond to nanoplastics as opposed to natural structures.

These results illustrate the real challenge of identifying nanoplastics particles in plant tissues and reinforces the interest of the approaches we have developed using Pd-doped nanoplastics and Pd measurement by ICP-MS, as well as the need to further develop advanced nanometrology techniques to eventually confidently measure nanoplastics without the aid of a tracer. The

approach used in the present study can be applicable to study other plant species as well as other organisms. I.e Pd-doped nanoplastics have been successfully applied to investigate the transport of nanoplastics in salmon gut sac ex vivo(Clark et al., 2022) and the uptake and egestion of nanoplastics by freshwater amphipod (Redondo-Hasselerharm et al., 2021) and earthworms (Lahive et al., 2022). Other polymers as well as other plastic morphologies with environmental relevance, such as fibers, can be envisaged as well (Frehland et al., 2020; Keller et al., 2020; Lahive et al., 2021; Mitrano et al., 2019).

3.4. Towards understanding impacts of nanoplastics exposure to wheat plants

This study highlights the potential of nanoplastics to be absorbed and transported to the aerial parts of wheat. Further studies should be conducted to evaluate the possible transfer of nanoplastics to the grains. In addition, we have shown important impacts on the cell walls (biochemical and structural) of exposed plants that are translated in changes in the root anatomy. Finally, we have shown the role of root exudates and mucilage in determining the behaviour of nanoplastics in the growth media. Further studies on exudation rates and composition for plants exposed to nanoplastics would help to better understand phytotoxicity and tolerance mechanisms in plants and would be a key in understanding the behaviour of nanoplastics in the growth media. This study highlights the need to explore new biomarkers and biological responses when exposed to a new type of pollutant (i.e. nanoplastics in this case). This may be applicable for other biological models and ecotoxicological studies in general, with the ultimate goal of establishing the most appropriate standard end points to allow for the comparison amongst different studies.

This study successfully demonstrated the potential of doped nanoplastics to trace nanoplastics in a simplified system. Following this proof of concept, further research should head towards more environmentally realistic conditions. First, the use of hydroponic system allowed to decouple the effects of the growth environment from the impacts of particulate plastic itself, but it is not representative of the complex soil environment. Further studies should be conducted to test whether plant uptake and translocation of nanoplastics also occurs in plants grown in soils. Second, concerning the dose, there is insufficient data on nano and microplastics concentrations in agricultural soils, so the method applied in this study should be tested over a wider range of concentration to cover the potential range of concentrations in soils. Third, pristine nanoplastics of only one type of polymer and size and two different morphologies have been tested. In summary, future research on nanoplastics-plant interactions should move to soil and long-term experiments to assess the real risk in terms of trophic transfer and crop production but still aim to understand the mechanisms which are responsible for uptake and impacts. This implies that better categorization of particle characteristics is needed to delineate their role in particle behaviour, i.e. polymer type and presence of additives, size and surface charge and heteroaggregation within the soil matrix. The study of uptake and transport routes in plant and the systematic study of soil characteristics influencing these processes must therefore still be considered. We anticipate that the aging process(es) of nanoplastics in the dynamic plant-soil system in which soil components and plant rhizosphere would strongly determine the fate of nanoplastics.

Considering the worldwide context of advancing agricultural practices with an increasing human population, the development of more efficient practices will be paramount to ensure a safe food

supply while optimizing resources and minimizing pollution. These developments are expected to strongly rely on the use of plastics both in greenhouses and in the fields, such as mulch films. Further plastic burdens on agricultural fields may be expected with the application of sewage sludge as organic fertilizer. It is therefore urgent to increase our knowledge about the impact of the presence of plastic residues and notably, nano and microplastics in agricultural systems. This study provides a foundation on the applicability of using metal-doped nanoplastics and adapted analytical tools to study the fate of nanoplastics in agricultural systems.

Acknowledgements

A.E.P.R thanks Atracción de Talento Program from Comunidad de Madrid and project SINCROPLANT (FP19 IMIDRA). D.M.M was funded through the Swiss National Science Foundation (grant numbers PZP002_168105 and PCEFP2_186856). We thank the French program LabEx Serenade (ANR-11-LABX-0064) for providing a fellowship to M.W and the French program EquipEx NanoID (ANR-10-EQPX-0039) for providing access to the MATRIX platform for sample preparation by CPD in CEREGE. Electron microscopy was performed at the CMTC characterization platform of Grenoble INP supported by the Centre of Excellence of Multifunctional Architectured Materials "CEMAM" n°AN-10-LABX-44-01 funded by the "Investments for the Future" Program. ISTerre is part of Labex OSUG@2020 (ANR10 LABX56).

We thank the ESRF committee for the provision of beamtime on ID19 through grant number ev-347, the assistance of the local contact Yin Cheng and Vincent Fernández from London Natural History Museum for his support during the experiment. The beamline team of ID16b and ID21 (ESRF) are acknowledged for providing inhouse beamtime. We thank Roxane Calais for her assistance in preliminary experiments and the ESRF traineeships program for providing her master student fellowship. We thank Perrine Chaurand from CEREGE (Aix en Provence, France) Rachel Martin from CMTC (Grenoble, France), and the staff of the geochemistry-mineralogy platform of ISTerre (Grenoble, France) for their technical support.

Author contributions

A.E.P.R conceived the study, was involved in the acquisition of µCT and µXRF data, participated in the analysis and interpretation of data and wrote the manuscript. D.M.M contributed to the conception of the study, provided the nanoplastics, was involved in the acquisition of µCT data, performed ICP-MS analysis and the leaching experiment and contributed to the manuscript writing. H.C contributed to the conception of the study, was involved in the acquisition of µCT and µXRF data, participated in data analysis and contributed to the manuscript writing. M.W conducted the plant experiment, the analysis of phytotoxicity markers and the acquisition of ATR-FTIR spectra. J.R.H developed the methodology for the analysis of ATR-FTIR. E.B and B.H analysed the µCT data, wrote the corresponding methods section and revised the manuscript. J.V performed the acquisition of nanoCT data and the 3D reconstructions. G.S conceived the study, supervised the plant experiment, was involved in the acquisition of µCT data, performed the SEM analysis, and contributed to write the manuscript. All the authors have given approval to the final version of the manuscript.

Competing interests

The authors declare no competing interests.

Figures

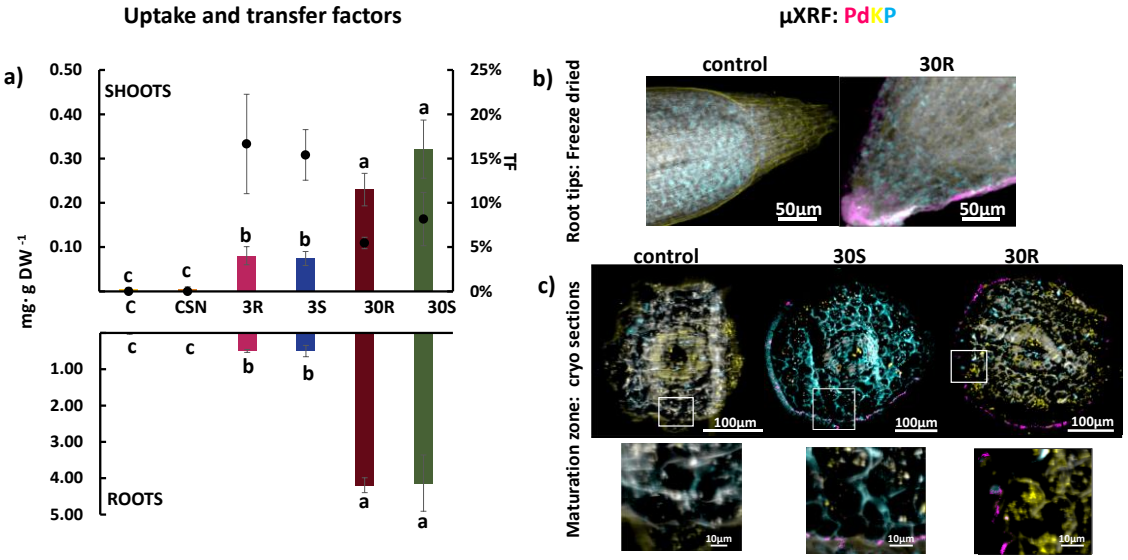

Figure 1: a) Nanoplastics concentration in shoots and roots. Bars are average nanoplastics concentration (mg·gDW^{-1}) (N=4), error bars are standard deviations. Different letters mean significant differences among treatments (Tukey test at $p \leq 0.05$). Points are transfer factor (%). µXRF tricolor maps showing the distribution of Pd (pink), K (yellow) and P (blue) of freeze-dried root tips b) and cryogenic root cross section of maturation zone.

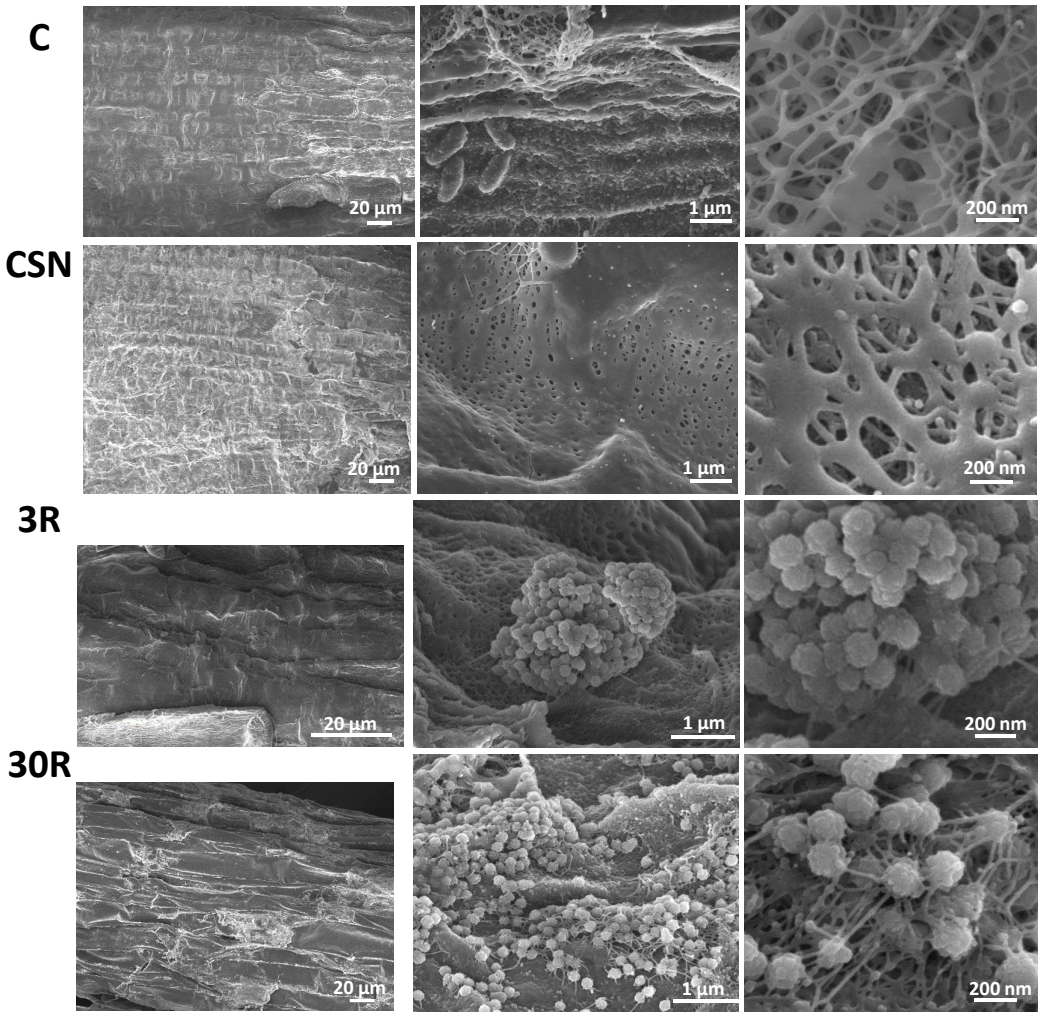

684

685 **Figure2: SEM observations of the root surface, 400 µm from the apex, for plants exposed to raspberry**
686 **nanoplastics. Nanoplastics are agglomerated and associated with polysaccharide filaments.**

687

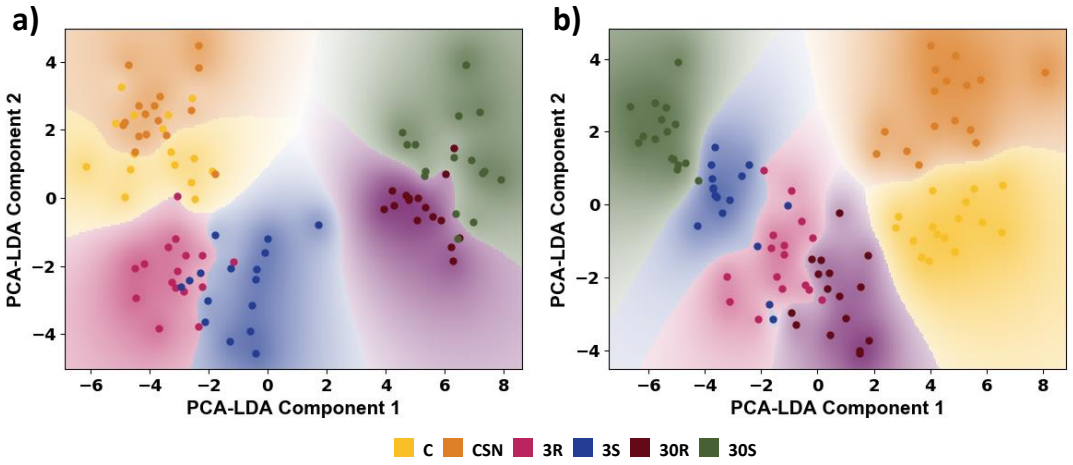

688

689 **Figure 3: PCA-LDA of the ATR-FTIR spectra collected from roots a) and shoots b). Four biological replicates per**
690 **treatment(n=4), with four technical replicates performed for each biological sample.**

691

692

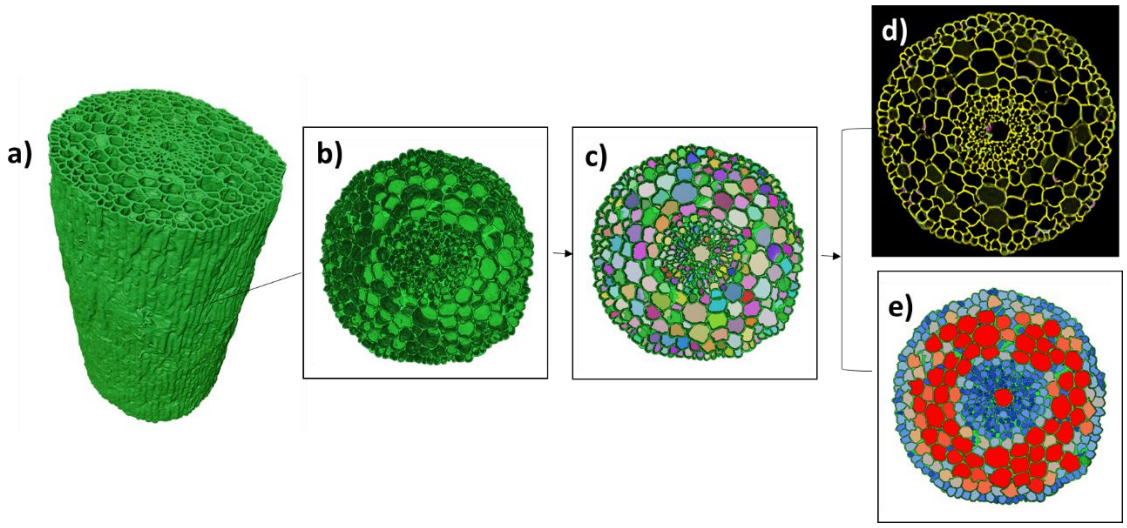

Figure 4: Impacts of nano-plastic on root architecture studied by synchrotron µCT with phase contrast: a) 3D rendering showing cell walls, b) rendering along Z-axis of the cell walls, c) virtual section through the 3D volume of the segmented cell walls and the labelled cell volumes, d) virtual slice (average of 20µm along Z-axis) through the 3D volume showing the distribution of high (magenta), medium (yellow) and low(cyan) cell wall density regimes, e) virtual slice showing cell walls and color-coded volumes from small (blue) to large(red). Allocations of cells according to regions of interest /epidermis, cortex and stele can be done based on their size and location.

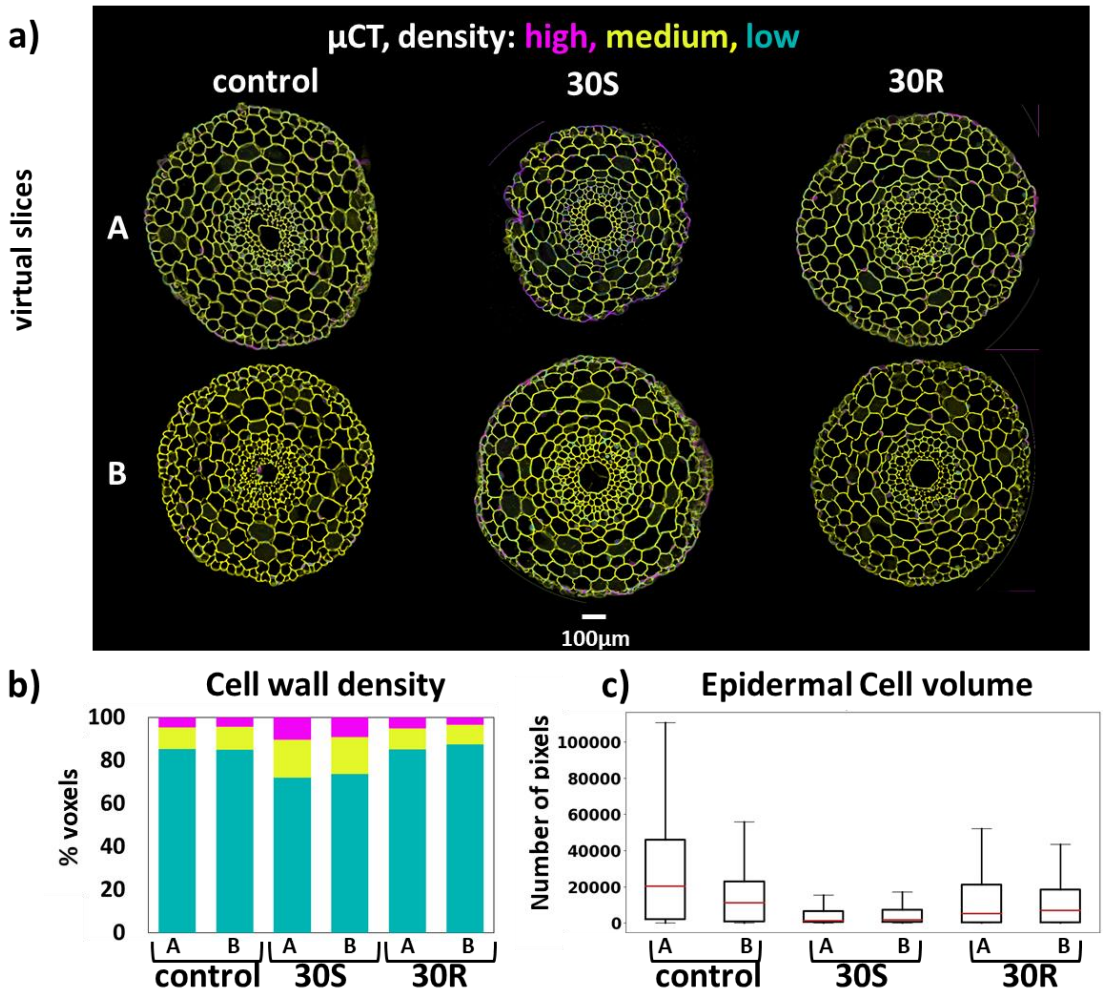

703

704 **Figure 5. Impacts on root architecture studied by synchrotron µCT with phase contrast (n=2): a) distribution of high**
705 **(magenta), medium (yellow) and low (cyan) cell wall density regimes in a virtual root slice (20µm), b) proportion of**
706 **voxels in each cell wall density regime, c) boxplot showing epidermal cell volume: box shows interquartile range**
707 **(IQR) Q1 to Q3, the red line is the median, whiskers show maximum and minimum (1.5 x IQR), outliers are not**
708 **shown.**

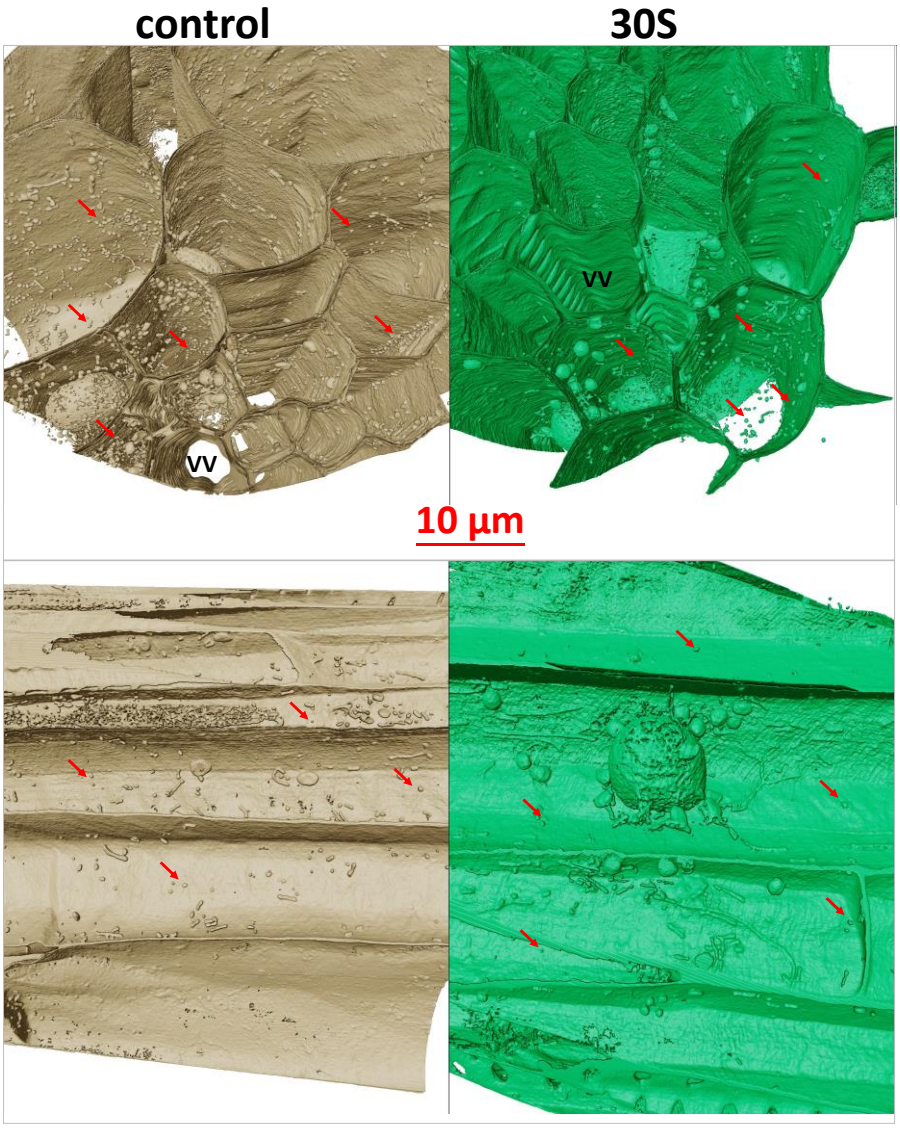

Figure 6: Analysis of roots by synchrotron nanoCT with phase contrast (n=1). 3D rendering of control root (brown) and root exposed to 30 mg·L^{-1} smooth nanoplastics (green) showing cortex cells and vasculature vessels (VV). Red arrows show particle-like structure with size lower than one micron. Full views are shown in Supplementary figure 18.

References

Avellan, A., Schwab, F., Masion, A., Chaurand, P., Borschneck, D., Vidal, V., Rose, J., Santaella, C., Levard, C., 2017. Nanoparticle Uptake in Plants: Gold Nanomaterial Localized in Roots of Arabidopsis thaliana by X-ray Computed Nanotomography and Hyperspectral Imaging. Environ. Sci. Technol. 51, 8682–8691. https://doi.org/10.1021/acs.est.7b01133

Bakshi, M., Liné, C., Bedolla, D.E., Stein, R.J., Kaegi, R., Sarret, G., del Real, A.E.P., Castillo-Michel, H., Abhilash, P.C., Larue, C., 2019. Assessing the impacts of sewage sludge amendment containing nano-TiO2 on tomato plants: a life cycle study. J. Hazard. Mater. https://doi.org/10.1016/J.JHAZMAT.2019.02.036

Bergmann, M., Mützel, S., Primpke, S., Tekman, M.B., Trachsel, J., Gerdts, G., 2019. White and wonderful? Microplastics prevail in snow from the Alps to the Arctic. Sci. Adv. 5, 1–11. https://doi.org/10.1126/sciadv.aax1157

Bradford, M.M., 1976. A rapid and sensitive method for the quantitation of microgram quantities of protein utilizing the principle of protein-dye binding. Anal. Biochem. 72, 248–254. https://doi.org/10.1006/abio.1976.9999

Brahmi, I., Mabrouk, Y., Brun, G., Delavault, P., Belhadj, O., Simier, P., 2016. Phenotypical and biochemical characterisation of resistance for parasitic weed (Orobanche foetida Poir.) in radiation-mutagenised mutants of chickpea. Pest Manag. Sci. 72, 2330–2338. https://doi.org/10.1002/ps.4278

Brinton, W.F., 2005. Characterization of man-made foreign matter and its presence in multiple size fractions from mixed waste composting. Compost Sci. Util. 13, 274–280. https://doi.org/10.1080/1065657X.2005.10702251

Canteri, M.H.G., Renard, C.M.G.C., Le Bourvellec, C., Bureau, S., 2019. ATR-FTIR spectroscopy to determine cell wall composition: Application on a large diversity of fruits and vegetables. Carbohydr. Polym. 212, 186–196. https://doi.org/10.1016/j.carbpol.2019.02.021

Castilleux, R., Plancot, B., Ropitaux, M., Carreras, A., Leprince, J., Boulogne, I., Follet-Gueye, M.L., Popper, Z.A., Driouich, A., Vicré, M., 2018. Cell wall extensins in root-microbe interactions and root secretions. J. Exp. Bot. 69, 4235–4247. https://doi.org/10.1093/jxb/ery238

Castillo-Michel, H.A., Larue, C., Pradas del Real, A.E., Cotte, M., Sarret, G., 2017. Practical review on the use of synchrotron based micro- and nano- X-ray fluorescence mapping and X-ray absorption spectroscopy to investigate the interactions between plants and engineered nanomaterials. Plant Physiol. Biochem. 110, 13–32. https://doi.org/10.1016/j.plaphy.2016.07.018

Chae, Y., An, Y.-J., 2020. Nanoplastic ingestion induces behavioral disorders in terrestrial snails: trophic transfer effect via vascular plants. Environ. Sci. Nano. https://doi.org/10.1039/c9en01335k

Chae, Y., An, Y.J., 2018. Current research trends on plastic pollution and ecological impacts on the soil ecosystem: A review. Environ. Pollut. 240, 387–395. https://doi.org/10.1016/j.envpol.2018.05.008

Chaudhry, Q., Blom-Zandstra, M., Gupta, S., Joner, E.J., 2005. Utilising the synergy between plants and rhizosphere microorganisms to enhance breakdown of organic pollutants in

768 the environment. Environ. Sci. Pollut. Res. 12, 34–48.
769 https://doi.org/10.1065/espr2004.08.213

770 Chen, Y., Leng, Y., Liu, X., Wang, J., 2020. Microplastic pollution in vegetable farmlands of
771 suburb Wuhan ,. Environ. Pollut. 257, 113449.
772 https://doi.org/10.1016/j.envpol.2019.113449

773 Clark, N.J., Khan, F.R., Mitrano, D.M., Boyle, D., Thompson, R.C., 2022. Demonstrating the
774 translocation of nanoplastics across the fish intestine using palladium-doped polystyrene
775 in a salmon gut-sac. Environ. Int. 159, 106994.
776 https://doi.org/10.1016/j.envint.2021.106994

777 Cloetens, P., Ludwig, W., Baruchel, J., Van Dyck, D., Van Landuyt, J., Guigay, J.P., Schlenker, M.,
778 1999. Holotomography: Quantitative phase tomography with micrometer resolution
779 using hard synchrotron radiation x rays. Appl. Phys. Lett. 75, 2912–2914.
780 https://doi.org/10.1063/1.125225

781 Corradini, F., Meza, P., Eguiluz, R., Casado, F., Huerta-Lwanga, E., Geissen, V., 2019. Evidence of
782 microplastic accumulation in agricultural soils from sewage sludge disposal. Sci. Total
783 Environ. 671, 411–420. https://doi.org/10.1016/j.scitotenv.2019.03.368

784 de la Fuente Cantó, C., Simonin, M., King, E., Moulin, L., Bennett, M.J., Castrillo, G., Laplaze, L.,
785 2020. An extended root phenotype: the rhizosphere, its formation and impacts on plant
786 fitness. Plant J. 103, 951–964. https://doi.org/10.1111/tpj.14781

787 Demšar, J., Curk, T., Erjavec, A., Gorup, Č., Hočevar, T., Milutinovič, M., Možina, M., Polajnar,
788 M., Toplak, M., Starič, A., Štajdohar, M., Umek, L., Žagar, L., Žbontar, J., Žitnik, M., Zupan,
789 B., 2013. Orange: Data Mining Toolbox in Python. J. Mach. Learn. Res. 14, 2349–2353.

790 Dhondt, S., 2012. Imaging as a tool to study leaf development in Arabidopsis thaliana.
791 (Doctoral dissertation, Ghent University)

792 Dong, J., Mao, W.H., Zhang, G.P., Wu, F.B., Cai, Y., 2007. Root excretion and plant tolerance to
793 cadmium toxicity - A review. Plant, Soil Environ. 53, 193–200.
794 https://doi.org/10.17221/2205-pse

795 Dong, Y., Gao, M., Qiu, W., Song, Z., 2021. Uptake of microplastics by carrots in presence of As
796 (III): Combined toxic effects. J. Hazard. Mater. 411, 125055.
797 https://doi.org/10.1016/j.jhazmat.2021.125055

798 Fakour, H., Lo, S., Yoashi, N.T., Massao, A.M., Lema, N.N., Mkhontfo, F.B., Jomalema, P.C.,
799 Jumanne, N.S., Mbuya, B.H., Mtweve, J.T., Imani, M., 2021. Quantification and Analysis of
800 Microplastics in Farmland Soils : Characterization , Sources , and Pathways. Agriculture
801 11, 330. https://doi.org/https://doi.org/10.3390/agriculture11040330

802 Feng, R., Lei, L., Su, J., Zhang, R., Zhu, Y., Chen, W., Wang, L., Wang, R., Dai, J., Lin, Z., 2020.
803 Toxicity of different forms of antimony to rice plant: Effects on root exudates, cell wall
804 components, endogenous hormones and antioxidant system. Sci. Total Environ. 711,
805 134589. https://doi.org/https://doi.org/10.1016/j.scitotenv.2019.134589

806 Frehland, S., Kaegi, R., Hufenus, R., Mitrano, D.M., 2020. Long-term assessment of nanoplastic
807 particle and microplastic fi ber fl ux through a pilot wastewater treatment plant using
808 metal-doped plastics. Water Res. 182, 115860.
809 https://doi.org/10.1016/j.watres.2020.115860

810 Freschet, G.T., Roumet, C., Comas, L.H., Weemstra, M., Bengough, A.G., Rewald, B., Bardgett,
811 R.D., De Deyn, G.B., Johnson, D., Klimešová, J., Lukac, M., McCormack, M.L., Meier, I.C.,

Pagès, L., Poorter, H., Prieto, I., Wurzburger, N., Zadworny, M., Bagniewska-Zadworna, A., Blancaflor, E.B., Brunner, I., Gessler, A., Hobbie, S.E., Iversen, C.M., Mommer, L., Picon-Cochard, C., Postma, J.A., Rose, L., Ryser, P., Scherer-Lorenzen, M., Soudzilovskaia, N.A., Sun, T., Valverde-Barrantes, O.J., Weigelt, A., York, L.M., Stokes, A., 2021. Root traits as drivers of plant and ecosystem functioning: current understanding, pitfalls and future research needs. New Phytol. https://doi.org/10.1111/nph.17072

Fuller, S., Gautam, A., 2016. A Procedure for Measuring Microplastics using Pressurized Fluid Extraction. Environ. Sci. Technol. 50, 5774–5780. https://doi.org/10.1021/acs.est.6b00816

Gantar, M., Rowell, P., Kerby, N.W., Sutherland, I.W., 1995. Role of extracellular polysaccharide in the colonization of wheat (Triticum vulgare L.) roots by N2-fixing cyanobacteria. Biol. Fertil. Soils 19, 41–48. https://doi.org/10.1007/BF00336345

Gao, W., Schlüter, S., Blaser, S.R.G.A., Shen, J., Vetterlein, D., 2019. A shape-based method for automatic and rapid segmentation of roots in soil from X-ray computed tomography images: Rootine. Plant Soil 441, 643–655. https://doi.org/10.1007/s11104-019-04053-6

Geyer, R., Jambeck, J.R., Law, K.L., 2017. Production , use , and fate of all plastics ever made. Sci. Adv. 25–29. https://doi.org/DOI: 10.1126/sciadv.1700782

Giorgetti, L., Spanò, C., Muccifora, S., Bottega, S., Barbieri, F., Bellani, L., Ruffini Castiglione, M., 2020. Exploring the interaction between polystyrene nanoplastics and Allium cepa during germination: Internalization in root cells, induction of toxicity and oxidative stress. Plant Physiol. Biochem. 149, 170–177. https://doi.org/10.1016/j.plaphy.2020.02.014

Heath, R.L., Packer, L., 1968. Photoperoxidation in isolated chloroplasts. Arch. Biochem. Biophys. 125, 189–198. https://doi.org/10.1016/0003-9861(68)90654-1

Horton, A.A., Walton, A., Spurgeon, D.J., Lahive, E., Svendsen, C., 2017. Microplastics in freshwater and terrestrial environments: Evaluating the current understanding to identify the knowledge gaps and future research priorities. Sci. Total Environ. 586, 127–141. https://doi.org/10.1016/j.scitotenv.2017.01.190

Jiang, X., Chen, H., Liao, Y., Ye, Z., Li, M., 2019. Ecotoxicity and genotoxicity of polystyrene microplastics on higher plant Vicia faba. Environ. Pollut. 250, 831–838. https://doi.org/10.1016/j.envpol.2019.04.055

Kanter, D.R., Musumba, M., Wood, S.L.R., Palm, C., Antle, J., Balvanera, P., Dale, V.H., Havlik, P., Kline, K.L., Scholes, R.J., Thornton, P., Tittonell, P., Andelman, S., 2018. Evaluating agricultural trade-offs in the age of sustainable development. Agric. Syst. 163, 73–88. https://doi.org/10.1016/j.agsy.2016.09.010

Kelessidis, A., Stasinakis, A.S., 2012. Comparative study of the methods used for treatment and final disposal of sewage sludge in European countries. Waste Manag. 32, 1186–1195. https://doi.org/10.1016/j.wasman.2012.01.012

Keller, A.S., Jimenez-Martinez, J., Mitrano, D.M., 2020. Transport of Nano- And Microplastic through Unsaturated Porous Media from Sewage Sludge Application. Environ. Sci. Technol. 54, 911–920. https://doi.org/10.1021/acs.est.9b06483

Krzesłowska, M., 2011. The cell wall in plant cell response to trace metals: Polysaccharide remodeling and its role in defense strategy. Acta Physiol. Plant. 33, 35–51. https://doi.org/10.1007/s11738-010-0581-z

Lahive, E., Cross, R., Saarloos, A.I., Horton, A.A., Svendsen, C., Hufenus, R., Mitrano, D.M.,

2022. Earthworms ingest microplastic fibres and nanoplastics with effects on egestion rate and long-term retention. Sci. Total Environ. 807, 151022. https://doi.org/10.1016/j.scitotenv.2021.151022

Lambert, S., Wagner, M., 2016. Characterisation of nanoplastics during the degradation of polystyrene. Chemosphere 145, 265–268. https://doi.org/10.1016/j.chemosphere.2015.11.078

Larue, C., Castillo-Michel, H., Sobanska, S., Cécillon, L., Bureau, S., Barthès, V., Ouerdane, L., Carrière, M., Sarret, G., 2014. Foliar exposure of the crop Lactuca sativa to silver nanoparticles: Evidence for internalization and changes in Ag speciation. J. Hazard. Mater. 264, 98–106. https://doi.org/10.1016/j.jhazmat.2013.10.053

Larue, C., Sarret, G., Castillo-michel, H., Elena, A., 2021. A Critical Review on the Impacts of Nanoplastics and Microplastics on Aquatic and Terrestrial Photosynthetic Organisms 2005834, 1–28. https://doi.org/10.1002/smll.202005834

Le Gall, H., Philippe, F., Domon, J.M., Gillet, F., Pelloux, J., Rayon, C., 2015. Cell wall metabolism in response to abiotic stress. Plants 4, 112–166. https://doi.org/10.3390/plants4010112

Li, C., Gao, Y., He, S., Chi, H., Li, Z., Zhou, X., Yan, B., 2021. Quanti fi cation of Nanoplastic Uptake in Cucumber Plants by Pyrolysis Gas Chromatography/Mass Spectrometry. https://doi.org/10.1021/acs.estlett.1c00369

Li, L., Luo, Y., Li, R., Zhou, Q., Peijnenburg, W.J.G.M., Yin, N., Yang, J., Tu, C., Zhang, Y., 2020. Effective uptake of submicrometre plastics by crop plants via a crack-entry mode. Nat. Sustain. https://doi.org/10.1038/s41893-020-0567-9

Lian, J., Liu, W., Meng, L., Wu, J., Chao, L., Zeb, A., Sun, Y., 2021. Foliar-applied polystyrene nanoplastics (PSNPs) reduce the growth and nutritional quality of lettuce (Lactuca sativa L.). Environ. Pollut. 280, 116978. https://doi.org/10.1016/j.envpol.2021.116978

Lian, J., Wu, J., Xiong, H., Zeb, A., Yang, T., Su, X., Su, L., Liu, W., 2020. Impact of polystyrene nanoplastics (PSNPs) on seed germination and seedling growth of wheat (Triticum aestivum L.). J. Hazard. Mater. 385, 121620. https://doi.org/10.1016/j.jhazmat.2019.121620

Liné, C., Manent, F., Wolinski, A., Flahaut, E., Larue, C., 2021. Comparative study of response of four crop species exposed to carbon nanotube contamination in soil. Chemosphere 274, 129854. https://doi.org/10.1016/j.chemosphere.2021.129854

Liu, Y., Guo, R., Zhang, S., Sun, Y., Wang, F., 2022. Uptake and translocation of nano / microplastics by rice seedlings : Evidence from a hydroponic experiment. J. Hazard. Mater. 421, 126700. https://doi.org/10.1016/j.jhazmat.2021.126700

Matos, A., Kerkhof, L., Garland, J.L., 2005. Effects of microbial community diversity on the survival of Pseudomonas aeruginosa in the wheat rhizosphere. Microb. Ecol. 49, 257–264. https://doi.org/10.1007/s00248-004-0179-3

Mirone, A., Brun, E., Gouillart, E., Tafforeau, P., Kieffer, J., 2014. The PyHST2 hybrid distributed code for high speed tomographic reconstruction with iterative reconstruction and a priori knowledge capabilities. Nucl. Instruments Methods Phys. Res. Sect. B Beam Interact. with Mater. Atoms 324, 41–48. https://doi.org/https://doi.org/10.1016/j.nimb.2013.09.030

Mitrano, Denise M., Beltzung, A., Frehland, S., Schmiedgruber, M., Cingolani, A., Schmidt, F., 2019. Synthesis of metal-doped nanoplastics and their utility to investigate fate and behaviour in complex environmental systems. Nat. Nanotechnol. 14, 362–368.

https://doi.org/10.1038/s41565-018-0360-3

Ng, E.L., Huerta Lwanga, E., Eldridge, S.M., Johnston, P., Hu, H.W., Geissen, V., Chen, D., 2018. An overview of microplastic and nanoplastic pollution in agroecosystems. Sci. Total Environ. 627, 1377–1388. https://doi.org/10.1016/j.scitotenv.2018.01.341

Piehl, S., Leibner, A., Löder, M.G.J., Laforsch, C., Bogner, C., 2018. Identification and quantification of macro- and microplastics on an agricultural farmland 1–9. https://doi.org/10.1038/s41598-018-36172-y

Pradas del Real, A.E., Silvan, J.M., de Pascual-Teresa, S., Guerrero, A., García-Gonzalo, P., Lobo, M.C., Pérez-Sanz, A., 2017a. Role of the polycarboxylic compounds in the response of Silene vulgaris to chromium. Environ. Sci. Pollut. Res. 24, 5746–5756. https://doi.org/10.1007/s11356-016-8218-4

Pradas del Real, A.E., Vidal, V., Carrière, M., Castillo-Michel, H., Levard, C., Chaurand, P., Sarret, G., 2017b. Silver Nanoparticles and Wheat Roots: A Complex Interplay. Environ. Sci. Technol. 51, 5774–5782. https://doi.org/10.1021/acs.est.7b00422

Redondo-Hasselerharm, P., Vink, G., Mitrano, D.M., Koelmans, A.A., 2021. Metal-doping of nanoplastics enables accurate assessment of uptake and effects on Gammarus pulex. Environ. Sci. Nano. https://doi.org/10.1039/d1en00068c

Rillig, M.C., Lehmann, A., 2020. Microplastic in terrestrial ecosystems. Science (80-.). 368, 1430. https://doi.org/DOI: 10.1126/science.abb5979

Rillig, M.C., Lehmann, A., de Souza Machado, A.A., Yang, G., 2019. Microplastic effects on plants. New Phytol. 223, 1066–1070. https://doi.org/10.1111/nph.15794

Savassa, S.M., Castillo-Michel, H., Pradas del Real, A.E., Reyes-Herrera, J., Marques, J.P.R., de Carvalho, H.W.P., 2021. Ag nanoparticles enhancingPhaseolus vulgarisseedling development: understanding nanoparticle migration and chemical transformation across the seed coat. Environ. Sci. Nano 8, 493–501. https://doi.org/10.1039/d0en00959h

Scheurer, M., Bigalke, M., 2018. Microplastics in Swiss Floodplain Soils. Environ. Sci. Technol. 52, 3591–3598. https://doi.org/10.1021/acs.est.7b06003

Schwab, F., Zhai, G., Kern, M., Turner, A., Schnoor, J.L., Wiesner, M.R., 2016. Barriers, pathways and processes for uptake, translocation and accumulation of nanomaterials in plants - Critical review. Nanotoxicology 10, 257–278. https://doi.org/10.3109/17435390.2015.1048326

Solé, V.A., Papillon, E., Cotte, M., Walter, P., Susini, J., 2007. A multiplatform code for the analysis of energy-dispersive X-ray f luorescence spectra. Spectrochim. Acta Part B At. Spectrosc. 62, 63–68. https://doi.org/10.1016/j.sab.2006.12.002

Song, X.Q., Liu, L.F., Jiang, Y.J., Zhang, B.C., Gao, Y.P., Liu, X.L., Lin, Q.S., Ling, H.Q., Zhou, Y.H., 2013. Disruption of secondary wall cellulose biosynthesis alters cadmium translocation and tolerance in rice plants. Mol. Plant 6, 768–780. https://doi.org/10.1093/mp/sst025

Steinmetz, Z., Wollmann, C., Schaefer, M., Buchmann, C., David, J., Tröger, J., Muñoz, K., Frör, O., Schaumann, G.E., 2016. Plastic mulching in agriculture. Trading short-term agronomic benefits for long-term soil degradation? Sci. Total Environ. 550, 690–705. https://doi.org/10.1016/j.scitotenv.2016.01.153

Sun, X.D., Yuan, X.Z., Jia, Y., Feng, L.J., Zhu, F.P., Dong, S.S., Liu, J., Kong, X., Tian, H., Duan, J.L., Ding, Z., Wang, S.G., Xing, B., 2020. Differentially charged nanoplastics demonstrate

distinct accumulation in Arabidopsis thaliana. Nat. Nanotechnol. 1–6. https://doi.org/10.1038/s41565-020-0707-4

Syberg, K., Khan, F.R., Selck, H., Palmqvist, A., Banta, G.T., Daley, J., Sano, L., Duhaime, M.B., 2015. Microplastics: Addressing ecological risk through lessons learned. Environ. Toxicol. Chem. 34, 945–953. https://doi.org/10.1002/etc.2914

Taylor, S.E., Pearce, C., Sanguinet, K., Hu, D., Chrisler, W.B., Kim, Y.-M., Wang, Z., Flury, M., 2020. Polystyrene Nano- and Microplastic Accumulation at Arabidopsis and Wheat Root Cap Cells, but No Evidence for Uptake into Roots. Environ. Sci. Nano. https://doi.org/10.1039/d0en00309c

Tran, T.M., MacIntyre, A., Hawes, M., Allen, C., 2016. Escaping underground nets: Extracellular DNases degrade plant extracellular traps and contribute to virulence of the plant pathogenic bacterium ralstonia solanacearum. PLoS Pathog. 12, 1–26. https://doi.org/10.1371/journal.ppat.1005686

Vandana, V. V., Suseela Bhai, R., Ramakrishnan Nair, R., Azeez, S., 2019. Role of cell wall and cell membrane integrity in imparting defense response against Phytophthora capsici in black pepper (Piper nigrum L.). Eur. J. Plant Pathol. 154, 359–375. https://doi.org/10.1007/s10658-018-01661-3

Wahl, A., Le Juge, C., Davranche, M., El Hadri, H., Grassl, B., Reynaud, S., Gigault, J., 2021. Nanoplastic occurrence in a soil amended with plastic debris. Chemosphere 262. https://doi.org/10.1016/j.chemosphere.2020.127784

Weithmann, N., Möller, J.N., Löder, M.G.J., Piehl, S., Laforsch, C., Freitag, R., 2018. Organic fertilizer as a vehicle for the entry of microplastic into the environment. Sci. Adv. 4, 1–8. https://doi.org/10.1126/sciadv.aap8060

Wu, X., Lu, J., Du, M., Xu, X., Beiyuan, J., Sarkar, B., Bolan, N., Xu, W., Xu, S., Chen, X., Wu, F., Wang, H., 2021. Particulate plastics-plant interaction in soil and its implications : A review. Sci. Total Environ. 792, 148337. https://doi.org/10.1016/j.scitotenv.2021.148337

Yin, L., Wen, X., Huang, D., Du, C., Deng, R., 2021. Interactions between microplastics / nanoplastics and vascular plants. Environ. Pollut. 290, 117999. https://doi.org/10.1016/j.envpol.2021.117999

Zhang, G.S., Liu, Y.F., 2018. The distribution of microplastics in soil aggregate fractions in southwestern China. Sci. Total Environ. 642, 12–20. https://doi.org/10.1016/j.scitotenv.2018.06.004

Zhang, T., Wang, C., Dong, F., Gao, Z., Zhang, C., 2019a. Uptake and Translocation of Styrene Maleic Anhydride Nanoparticles in Murraya Exotica Plants as Revealed by Noninvasive , Real-Time Optical Bioimaging. Env. Sci Technol 53, 1471–1481. https://doi.org/https://doi.org/10.1021/acs.est.8b05689

Zhang, T., Wang, C., Dong, F., Gao, Z., Zhang, C., Zhang, X., Fu, L., Wang, Y., Zhang, J., 2019b. Uptake and Translocation of Styrene Maleic Anhydride Nanoparticles in Murraya exotica Plants As Revealed by. Environ. Sci. Technol. 53, 1471–1481. https://doi.org/10.1021/acs.est.8b05689

Assessing implications of nanoplastics exposure to plants with advanced nanometrology techniques

Ana Elena Pradas del Real*[1,3], Denise M. Mitrano[2], Hiram Castillo-Michel[3], Mohammad Wazne[3,5], Juan Reyes-Herrera[3], Emely Bortel[4], Bernhard Hesse[3,4], Julie Villanova[3], Géraldine Sarret[5]

1 IMIDRA (Madrid Institute for Agroenvironmental Research). 28800 Alcalá de Henares. Spain

2 ETH Zurich, Universitatstrasse 16, 8092 Zurich, Switzerland

3 ESRF, The European Synchrotron, CS 4022038043 Grenoble Cedex 9, France

4 Xploraytion GmbH, Bismarckstrasse 10-12, 10625, Berlin, Germany

5 ISTerre (Institut des Sciences de la Terre), Univ. Grenoble Alpes, CNRS, 38000

Abstract

Despite the increasing attention given to the impacts of nanoplastics in terrestrial environments, there is limited data about the effects on plants, and the quantitative information on uptake. In the present study, wheat plants grown in hydroponics were exposed to Pd-doped nanoplastics. This allowed us to quantify nanoplastics uptake and translocation to the shoots. Visualization of nanoplastics in roots was performed with synchrotron micro X-ray fluorescence (μXRF). Nanoplastics accumulated on the root epidermis, especially at the root tip and in root maturation zones. A close relationship between plant roots, rhizodeposits and nanoplastics behaviour was shown. Reinforcement of the cell wall in roots was evidenced using Fourier transform infrared spectroscopy (FTIR) and synchrotron-computed microtomography (μCT). Synchrotron-computed nanotomography (nanoCT) evidenced the presence of globular structures but they could not be identified as nanoplastics since they were observed both in the control and treated roots. By utilizing the inorganic tracer in the doped-nanoplastics, this study paves the road for elucidating interactions in more complex systems by using an integrative approach combining classical phytotoxicity markers with advanced nanometrology techniques.